Spatiotemporal Trends in Near-Natural New Zealand River Flow

LAURA E. QUEEN,[a] SAM DEAN,[b] DÁITHÍ STONE,[b] RODDY HENDERSON,[b] AND JAMES RENWICK[a]

[a] *Victoria University of Wellington, Wellington, New Zealand*
[b] *National Institute of Water and Atmospheric Research, Wellington, New Zealand*

(Manuscript received 28 February 2022, in final form 27 October 2022)

ABSTRACT: Anthropogenic climate change is affecting rivers worldwide, threatening water availability and altering the risk of natural hazards. Understanding the pattern of regional streamflow trends can help to inform region-specific policies to mitigate and adapt to any negative impacts on society and the environment. We present a benchmark dataset of long, near-natural streamflow records across Aotearoa New Zealand (NZ) and the first nationwide analysis of observed spatiotemporal streamflow trends. Individual records rarely have significant trends, but when aggregated within homogenous hydrologic regions (determined through cluster analyses), significant regional trends emerge. A multitemporal approach that uses all available data for each region and considers trend significance over time reveals the influence of decadal variability in some seasons and regions, and consistent trends in others. Over the last 50+ years, winter streamflow has significantly increased in the west South Island and has significantly decreased in the north North Island; summer streamflow has significantly decreased for most of the North Island; autumn streamflow has generally dried nationwide; and spring streamflow has increased along the west coast and decreased along the east coast. Correlations between streamflow and dynamic and thermodynamic climate indices reveal the dominant drivers of hydrologic behavior across NZ. Consistencies between the observed near-natural streamflow trends and observed changes in circulation and thermodynamic processes suggest possible climate change impacts on NZ hydrology.

KEYWORDS: Rivers; Southern Hemisphere; Hydrologic cycle; Climate change

1. Introduction

Anthropogenic climate change is intensifying the variability of the water cycle (Douville et al. 2021), increasing the frequency and intensity of floods (Hirabayashi et al. 2013) and droughts (Trenberth et al. 2014) and threatening water availability around the world (Konapala et al. 2020). Global trends in observed mean and extreme river flow have been detected and attributed to anthropogenic climate change, emphasizing the pervasive effects of climate change on the water cycle and patterns of terrestrial hydrology (Gudmundsson et al. 2019, 2021; Milly et al. 2005). Streamflow, however, is inherently a small-scale process, influenced by local topography, soil type, land cover, weather, the interaction of groundwater, and human influences beyond emissions, such as water abstractions and river engineering (Jencso et al. 2009; Vörösmarty and Sahagian 2000; Winter 2001). Regional studies unpack the complexity of these small-scale processes to better to best inform communities and policymakers.

Rivers dominate the Aotearoa New Zealand (NZ) landscape, providing communities with drinking water, irrigation for agriculture and food production, and most of the nation's renewable electricity (Ministry of Business, Innovation and Employment 2021). Rivers further provide habitat for many endemic species and are central to the Māori mauri (life force). Understanding observed changes in NZ streamflow can help us anticipate future changes and inform policies to protect these environmental, cultural, and economic resources.

NZ is an ideal location to study the effects of global change on local-scale processes, as the hydroclimate system in NZ is dominantly defined by the interaction of large-scale circulation patterns and NZ's mountainous landscape (Mullan 1998; Salinger 1980). Along the South Island, the southern storm track collides with the Southern Alps, an extended mountain range that blocks much of the prevailing westerlies, causing orographic precipitation to douse the region west of the great divide and casting a rain shadow to the east (Henderson and Thompson 1999; Purdy and Austin 2003; Salinger 1980; Tait and Fitzharris 1998; Trenberth 1991). Atmospheric rivers within the wind belt play an essential role in rainfall and subsequent regional water resources, particularly along the west South Island (Prince et al. 2021; Shu et al. 2021). In the North Island, frontal systems and extratropical cyclones drive precipitation (Dravitzki and McGregor 2011; Tait and Fitzharris 1998).

Anthropogenic climate change is causing temperatures to rise and circulation patterns to shift across NZ, which may interact in complex ways to affect streamflow. For example, observed changes to the strength and position of the southern storm track have likely increased rainfall on the west coast of the South Island, and this should be detectable in river flow trends (Bender et al. 2012; Harrington and Renwick 2014; Yin 2005). Beyond circulation changes, temperatures have been observed and projected to rise across NZ due to climate

Denotes content that is immediately available upon publication as open access.

Supplemental information related to this paper is available at the Journals Online website: https://doi.org/10.1175/JHM-D-22-0037.s1.

Corresponding author: Laura E. Queen, laura.queen@vuw.ac.nz

DOI: 10.1175/JHM-D-22-0037.1

change (Dean and Stott 2009; Mullan 2012). Rising temperatures affect the timing and magnitude of snowfall and subsequent snowmelt, which may cause regime shifts in the snow-dominant catchments, including NZ's alpine regions (Zierl and Bugmann 2005).

A key to assessing observed trends in streamflow is considering spatial patterns, understanding how topography and other factors create regional streamflow characteristics. Even if many individual records do not have statistically significant trends, notable spatial patterns can emerge from a collection of apparently insignificant trends. Many studies generalize spatial patterns from local results (Lins and Slack 2005; Stahl et al. 2010), but some quantify the spatial dimension by assessing covariance within the streamflow network and aggregating records within regions to create a regional time series, thus reducing noise and amplifying any coherent trends within the region (Hannaford et al. 2013). The regionalization of climate variables across NZ is common, with widespread use of the climate regions defined by rotated empirical orthogonal function (EOF) analyses of observed temperature, rainfall, sea surface temperature, and mean sea level pressure (Mullan 1998; Salinger and Mullan 1999). We follow the philosophy of this practice by performing cluster analyses to assess trends regionally.

While observed changes in NZ streamflow have not been documented (Lawrence et al. 2022), a recent study assessed NZ hydroclimate behavior through the lens of emergence—when will the effects of climate change on future NZ river flow be detectable? (Collins 2021). Using a chain of climate and hydrologic models to simulate future river flow, Collins found that the strongest sentinel of climate change in NZ rivers is mean winter flow, particularly for the west coast of the South Island, with time of emergence in the midcentury or later under sustained anthropogenic forcing. Collins hypothesizes that winter is the strongest sentinel because winter contains both the lowest flows in this region and the highest trends due to increasing westerlies and warming temperatures shifting runoff from spring snowmelt to winter rainfall. Future projections of NZ river flow generally show flow increasing in the west and south and decreasing in the north and east, with the largest increases occurring in winter and the greatest decreases occurring in summer (Collins 2020).

Other human influences on the water cycle have increased simultaneously with climate change, such as land use change, water abstraction, and river engineering for flood management and hydroelectric power. Benchmark networks, such as the United Kingdom Benchmark Network (Harrigan et al. 2018) and the United States Hydro-Climatic Data Network (Slack and Landwehr 1992), have been established to assess long-term, climate-driven hydrologic variability and change such as changes to the occurrence and magnitude of floods or droughts and the seasonal distribution of water supplies (Hannaford et al. 2021; Lins and Slack 2005). Records in these networks are considered "near-natural" and are reasonably free from human disturbances outside of anthropogenic climate change. We have compiled a network of near-natural streamflow observations across NZ and analyzed the new benchmark dataset for spatiotemporal trends in seasonal streamflow. We explore potential drivers of hydrologic behavior across NZ by correlating the observed streamflow with dynamic and thermodynamic climate indices.

The paper is arranged as follows. Data sources and analysis techniques are described in section 2 and results are presented in section 3. The discussion of results and conclusions drawn are contained in section 4.

2. Data and methods

a. Observed streamflow network

To assess climate-driven changes in seasonal NZ streamflow, we compiled a network of observed flow records which are suitable for long-term trend analysis and are reasonably free from human influence. Catchments in the network are considered near-natural because their hydrologic behavior has not been influenced by land use change (i.e., deforestation, urbanization), water abstractions (i.e., irrigation), and river engineering such as dam infrastructure for flood management and hydroelectric production. Catchments are chosen based on the following criteria:

1) The total fraction of catchment flow consented for abstraction is less than 0.05.
2) The record is at least 50 years long and includes the years 1969–2019.
3) The catchment is not nested inside another catchment included in the network.
4) The record has high hydrometric data quality, i.e., no large gaps.

The network is representative of NZ's hydroclimate variability and includes 53 records (Fig. 1), including measured gauge sites and lake inflows. A table of metadata, geophysical properties, and hydroclimate characteristics for the catchments in the network can be found in the online supplemental material. The lake inflows are calculated from extremely accurate measures of outflow. Specifically, inflow is defined as gross inflow less surface evaporation and groundwater losses and obtained from the conservation of volume equation, inflow = outflow + (level change) × area/(time step) (Gilbert 1978). Over geological time, the lake outlets have become stable such that at each lake a constant relationship exists between the level and the outflow.

Twenty-five sites are in the North Island and 28 sites are in the South Island. The eight inflow sites are Lake Waikaremoana in the North Island and Lakes Ohau, Pukaki, Tekapo, Hawea, Wanaka, Te Anau, and Monowai in the South Island.

Seasonal means are calculated as an average of daily flow data within the defined seasons: winter (June–August), spring (September–November), summer (December–February), and autumn (March–May). Missing daily values are ignored in the calculation of a seasonal value, unless 1) more than 1/3 of the daily values are missing or 2) there are more than 7 consecutive days missing. If either apply, the entire season is considered missing.

b. Trend analysis

Temporal trends in streamflow are detected using the Mann–Kendall (MK) rank correlation statistical test (Kendall 1975;

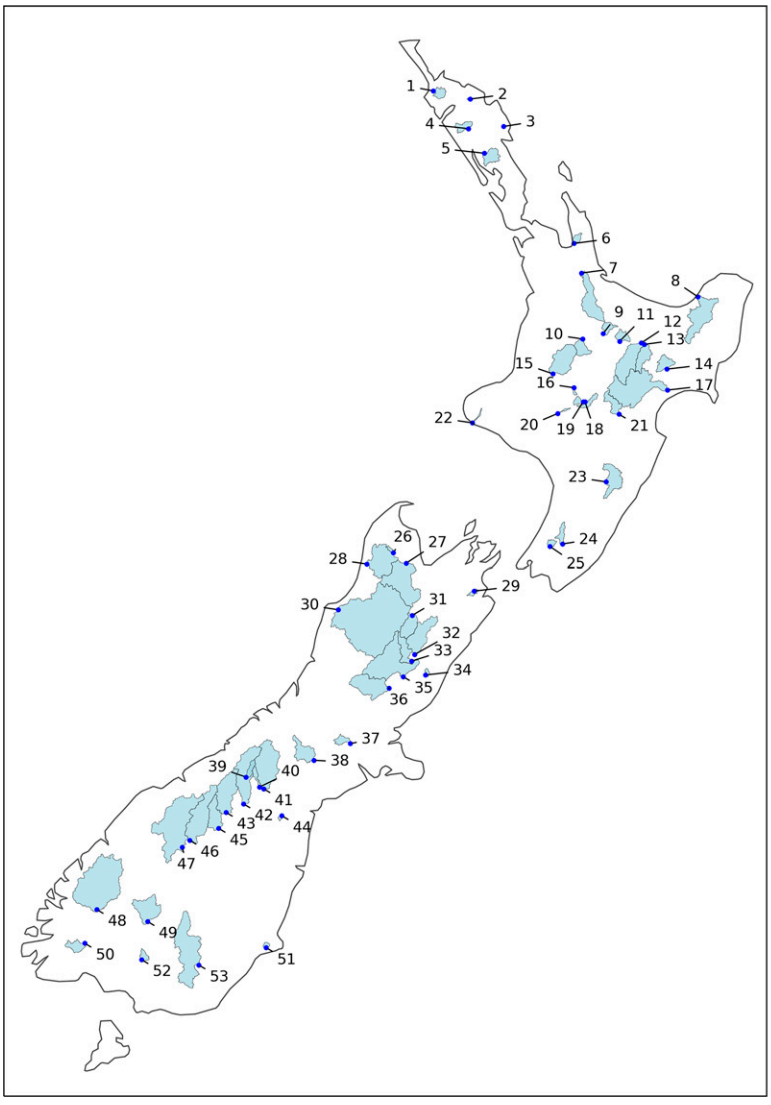

FIG. 1. Catchments included in the near-natural observed streamflow network.

Mann 1945). The MK test detects statistically significant monotonic trends by considering the number of concordant and discordant pairs in a series. The MK test is nonparametric, meaning the distributions of time and streamflow are not assumed. We use the MK test to detect trends and their statistical significance (p value) and Sen's slope (β) to estimate the magnitude of the trend for local and regional seasonal streamflow (Sen 1968) (methods described in appendix). The MK test and Sen's slope are frequently applied to estimate the statistical significance and magnitude of hydrologic trends (Aawar et al. 2019; Birsan et al. 2005, 2014; Burn 2008; Burn and Hag Elnur 2002; Chauluka et al. 2021; Chen et al. 2016; Dixon et al. 2006; Gautam and Acharya 2012; Gumus et al. 2022; Hu et al. 2020; Mallick et al. 2021; Nayak et al. 2010). We use the pyMannKendall python package (Hussain and Mahmud 2019) to estimate trend significance (p value) and magnitude (β). Because variability in NZ streamflow occurs on the order of weeks, we assume statistical independence across years.

Local trends are calculated on normalized streamflow (subtract the record's mean and divide by its standard deviation) over the shared 50-yr time window, 1969–2019. Regional trends are assessed with a multitemporal approach, considering both trends over a shared window and the maximum time periods for each region. The regional time series is the equally weighted average of the normalized individual records within the region and begins on the date that at least three records in the region are active. An example trend analysis for a single record (Fig. 2), the Whanganui River at Te Porere, shows scatterplots of the seasonal time series and a locally weighted regression curve (LOWESS) representing the smoothed trend (Seabold and Perktold 2010). The LOWESS fit estimates a value at each point by fitting a weighted least squares to a local subset, 1/3 of the full data, giving more weight to nearby points and less to distant points. The MK test and Sen's slope methods are applied to the seasonal time series and the

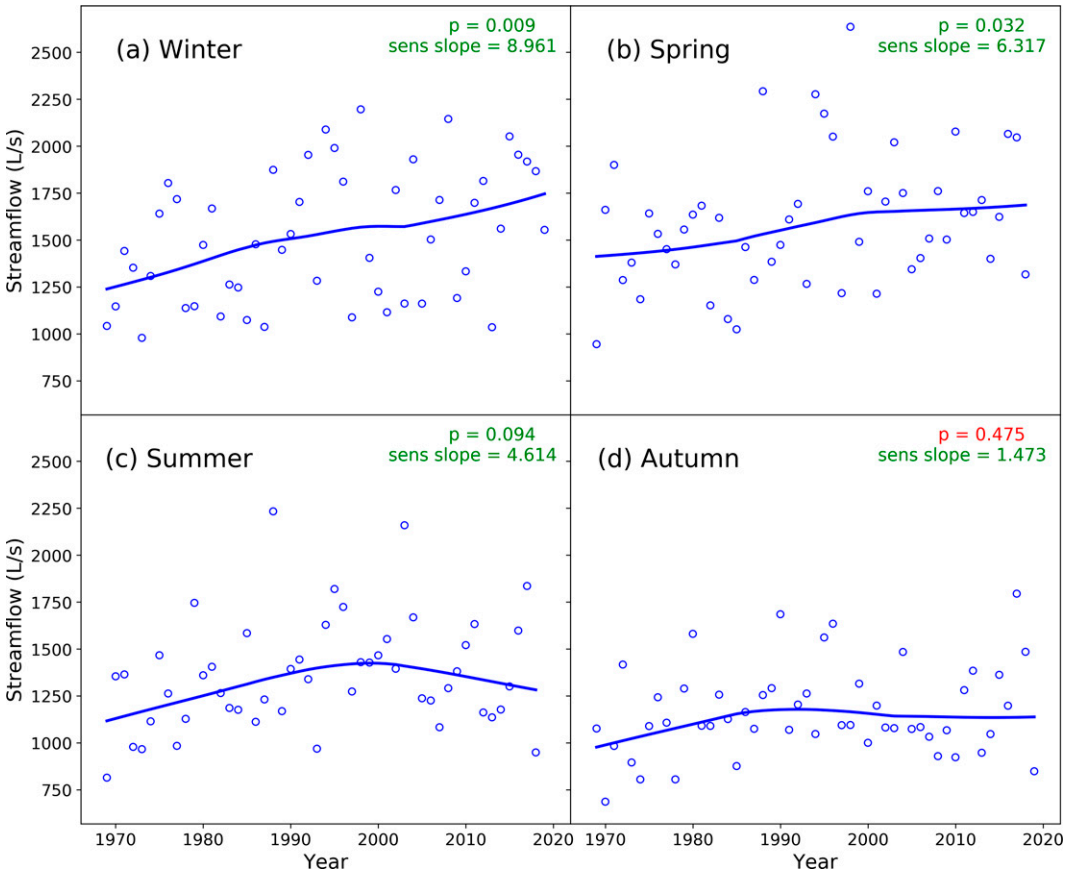

FIG. 2. Example seasonal streamflow time series of Whanganui River at Te Porere (33347) with LOWESS smoothing and Mann–Kendall p value and Sen's slope trend results. The font is colored red if p is greater than 0.1.

resultant β and p values are printed in the upper-right corner for each season.

c. *Regionalization*

To assess regional streamflow trends, we define regions of homogenous hydrologic behavior in terms of seasonal interannual variability through cluster analyses. We consider two methods to inform the definition of regions: self-organizing maps (SOM) and principal component analysis (PCA).

The SOM method is an unsupervised artificial neural network that clusters groups of similar input patterns from a high dimensional input space in a nonlinear fashion onto a low dimensional discrete lattice of neurons in an output layer (Kohonen 1990). Similarity between the input patterns is quantified by means of a distance measure, in this case Euclidian distance between seasonal time series. Neurons in the output layer are positioned such that closer neurons are more similar, allowing the neurons, and the input patterns they contain, to be clustered based on similarities and interdependencies. Specifics on the algorithm can be found in Kohonen (1990), and a review of the SOM method in hydrology is presented by Kalteh et al. (2008).

The main advantages of the SOM method are that it is nonlinear, it has an ability to preserve the topological structure of the data, and that the number of clusters is not determined a priori, but results from the process itself. Additionally, the SOM method is more precise than conventional hierarchical and partitional cluster methods which do require a predetermined number of clusters, such as the k-means or Ward's methods (Lin and Chen 2006). In previous studies, the SOM method has often been used for the estimation of ungauged catchments or flood frequency analysis, with input data varying from catchment descriptors (i.e., latitude, longitude, area, elevation), streamflow signatures (i.e., average discharge, standard deviation, percentiles), to raw streamflow time series depending on the use (Di Prinzio et al. 2011; Hsu and Li 2010; Lauzon et al. 2006; Ley et al. 2011; Sharghi et al. 2018; Toth 2013). As we are interested in defining broadly homogenous hydrologic regions based on seasonal interannual variability, we use normalized (the mean is subtracted, and the standard deviation is divided from each record) 50-yr seasonal streamflow time series, 1969–2019, as the input layer for the SOM algorithm. We implemented SOMs using various sizes of output layers (2×2, 3×3, 4×4) over many iterations to identify consistent regions of similar interannual streamflow variability for each season. While smoothing functions or parameterizations of raw time series are often used to reduce noise in the input layer, we successfully produced consistent regions with the time series normalized only, possibly due to the

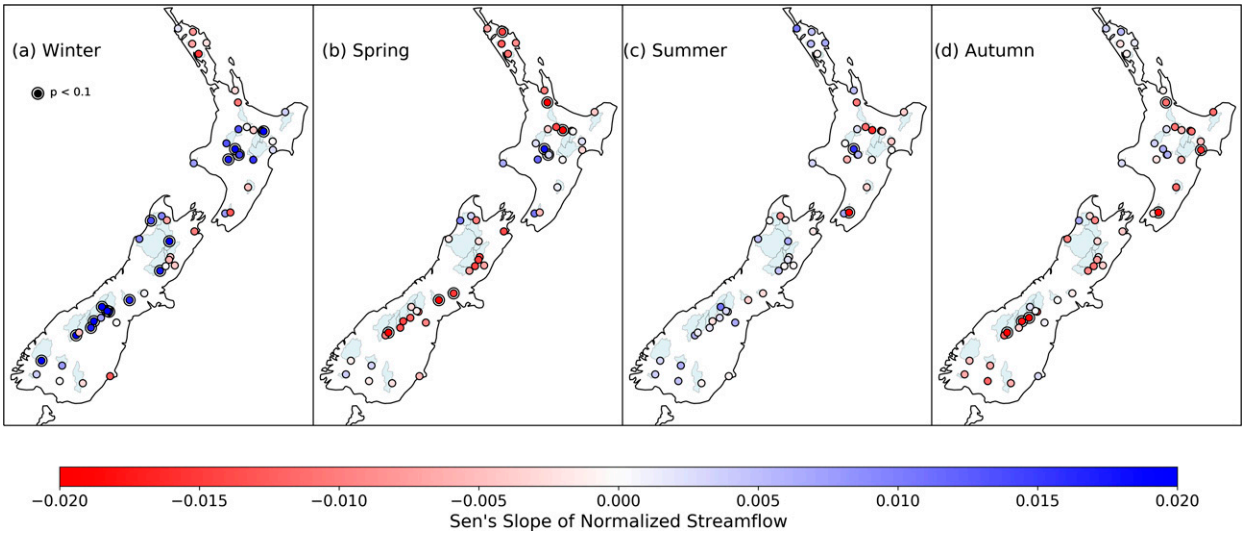

FIG. 3. Local Mann–Kendall trend results of normalized, seasonal streamflow over period 1969–2019, with trend magnitude (Sen's slope β) shown in color and statistical significance ($p < 0.1$) denoted with a double outlined marker.

strong control orography has on defining distinct hydrologic and climate regions in NZ (Mullan 1998). We use the python package SuSi to perform SOMs (Riese et al. 2020).

PCA identifies the main modes of spatial and temporal variability in a multidimensional dataset, sorted by the amount of variance they account for, and has been used extensively to detect hydrologically coherent regions (Guetter and Georgakakos 1993; Lins 1997; Maurer et al. 2004). The leading PCA spatial (empirical orthogonal function, EOF) pattern defines the combination of streamflow records to give the largest-variance amplitude time series [principal component (PC)]. The second EOF is the pattern that accounts for the largest amount of the remaining variance (and is orthogonal to the first EOF), and so on. For each season, regions are defined by the regionality of the leading EOF patterns.

d. Correlating to dynamic and thermodynamic indices

We correlate the observed streamflow records to various dynamic and thermodynamic indices from the ERA5 reanalysis to assess potential drivers of seasonal hydrologic behavior and change. Dynamic climate indices describe aspects of atmospheric circulation, while thermodynamic climate indices relate to the transfer of heat and energy in the Earth system. ERA5 is a state-of-the-art global reanalysis which provides estimates of atmospheric, land, and oceanic climate variables based on historic observations across the globe on a 30-km grid (Hersbach et al. 2020). ERA5 has previously been found to simulate precipitation well over NZ (Pirooz et al. 2021). We correlate 1969–2019 NZ streamflow with indices of ERA5 mean sea level pressure gradients, total precipitation, and snowfall. In the absence of adequate snow observations in NZ, we analyzed the annual cycle of ERA5 snowfall, snowmelt, rainfall, and runoff to further assess the role of snowmelt in NZ's alpine hydrology and provide an insight into ERA5 snow hydrology. Annual cycles of monthly ERA5 and observed streamflow time series are calculated over the period 1969–2019.

To relate the observed flow to patterns in atmospheric circulation, we calculate zonal (east–west) and meridional (north–south) wind indices, Z1 and M1, respectively, as defined by Trenberth (1976), by taking the difference in the mean sea level pressure time series at Auckland, NZ, minus Christchurch, NZ (Z1), and Hobart, Australia, minus Chatham Islands, NZ (M1). Circulation indices derived from ERA5 were found to correlate highly to those estimated from station pressure records (Z1 $r = 0.9$, $p = 0.0$; M1 $r = 0.9$, $p = 0.0$), and henceforth we use the ERA5 values only.

Correlations between observed streamflow, total precipitation, and snowfall are calculated for each record with ERA5 data first bilinearly interpolated to a 3-km grid and then masked by the catchment shape and averaged. All time series are detrended to assess the seasonal interannual correlations between the indices and streamflow and not the similarities in long-term trends. The catchment boundary information was not available for one small catchment in Northland, Ngunguru at Dougmore's Rock, so this record is not used in the correlation analysis. We use the Pearson's correlation implemented by Pandas python library (Reback et al. 2020).

3. Results

a. Local trends

Maps of 50-yr (1969–2019) seasonal trend results for individual records reveal locations of significant change and emerging spatial patterns of change across NZ (Fig. 3). Significance is measured at the $p < 0.1$ level. In winter, 15 records have statistically significant increasing trends: Whanganui at Te Porere, Lake Ohau at Lake Middleton, Jollie at Mt Cook Stn, Lake Wanaka at Roys Bay, Forks at Balmoral, Wairau at Dip Flat, Whirinaki at Galatea, Sth Ashburton at Mt Somers,

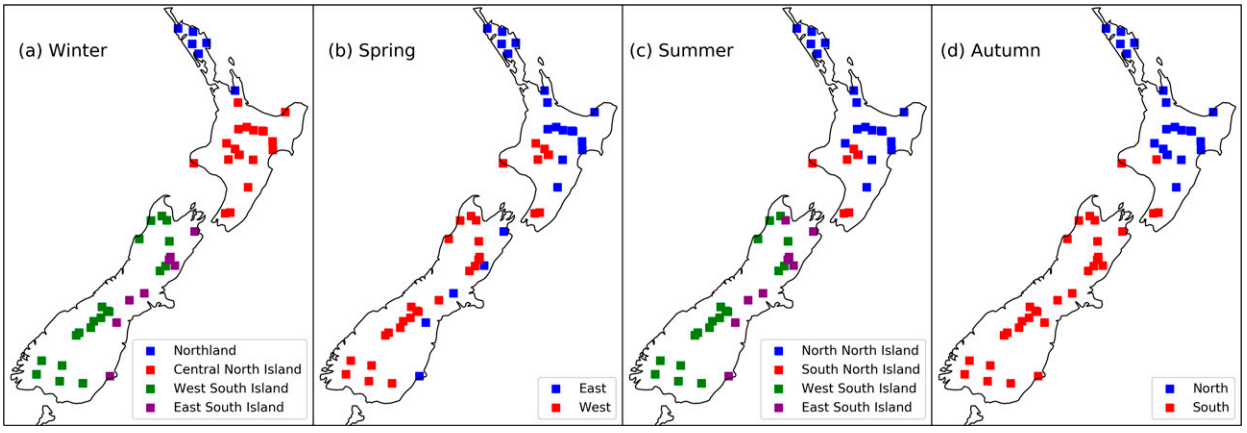

FIG. 4. Seasonal hydroclimate regions informed by SOMs and PCA cluster analyses on seasonal streamflow records 1969–2019.

Ahuriri at Sth Diadem, Lake Tekapo at Power Station Intake, Lake Te Anau at Park HQ, Waihohonu Stm at Desert Rd, Karamea at Arapito, Hurunui at Mandamus, Makotuku at SH49A Br. The greatest increases occur on the west of the South Island and the greatest decreases in north North Island. The emergent spatial pattern of winter trends shows increasing flows on the west South Island and central North Island and decreasing or stationary flows on the east South Island and north North Island.

In spring, most of the records have decreasing trends, with eight catchments significantly decreasing over the period: Waihou at Te Aroha Br, Whanganui at Te Porere, Sth Ashburton at Mt Somers, Lake Hawea at Dam, Waiotapu at Reporoa, Maungaparerua at Tyrees Ford, Selwyn at Whitecliffs, Waihohonu Stm at Desert Rd. Catchments in the central North Island are exceptions to the overall decreasing trend, where several catchments have increasing trends including Whanganui at Te Porere and Waihohonu Stm at Desert Rd which are significantly increasing.

Summer presents a more chaotic spatial pattern of local trends, with catchments sporadically showing increasing, decreasing, and nonexistent trends. Two catchments have significant trends, both in the North Island, Waiohine at Gorge and Whanganui at Te Porere, but many more catchments have near-zero trends compared to the other seasons.

Finally, autumn streamflow across the country has generally decreased, except for some northern and western catchments of the North Island. North Island trends are similar between summer and autumn, with increasing flow in the west and decreasing in the east. Six catchments have significantly decreased: Waiohine at Gorge, Lake Pukaki at Canal Inlet Gate, Waihou at Te Aroha Br, Lake Ohau at Lake Middleton, Lake Hawea at Dam, and Mohaka at Raupunga.

b. Regions

Figure 4 shows the seasonal regions of homogenous hydrologic behavior as informed by the consistent patterns which emerged from repeated SOMs and PCA cluster analyses. Homogenous regions encompass different numbers of sites and the agreement across sites differs between regions. Winter and summer have four regions, a west–east divide in the South Island and a north–south divide in the North Island. Spring and autumn have two regions, east and west, and north and south, respectively.

The projection of prevailing westerlies onto the Southern Alps is clear in the winter, summer, and spring maps as the mountains cast a rain shadow across the east South Island defining distinct regions of hydrologic behavior—wet in the west and dry in the east. Some catchments east of the divide are considered west coast catchments because they drain from the Southern Alps and are highly influenced by westerlies. A band of anticyclones bring settled weather to the northern reaches of the North Island defining a northern hydroclimate region which contains much of the North Island in the summer and is constrained to a smaller northern region in winter when the southern storm track expands northward (Nakamura and Shimpo 2004; Simmonds and Keay 2000; Trenberth 1991).

Figure 5 presents a closer look at the covariability of catchments in the South Island, grouping the catchments by annual cycle patterns. Figure 5a shows the central mountainous catchments, whose annual cycle pattern is highly influenced by snow, with flow minimized in the winter when water is stored as snowpack and peaked in the summer due to the combination of rainfall and snowmelt. Figure 5c comprises the west South Island catchments which are influenced by the seasonal behavior of the southern storm track with flow peaking in the autumn and spring. This may be due to the southern semiannual oscillation which brings stronger temperature gradients across NZ and thus stronger westerlies in the spring and autumn; the larger peak in spring is possibly due to the combination of stronger westerlies and snowmelt (Ackerley and Renwick 2010; Nakamura and Shimpo 2004; Simmonds and Keay 2000; Trenberth 1991). Figure 5b shows the annual cycle of the eastern South Island catchments, which have either a single peak in early winter (central Orago catchments), midwinter (northern east coast catchments), or consistent flow throughout the year (southern east coast catchments).

c. Regional trends

Figure 6 shows regional trends for each season based on the regional time series over the shared time window, 1969–2019.

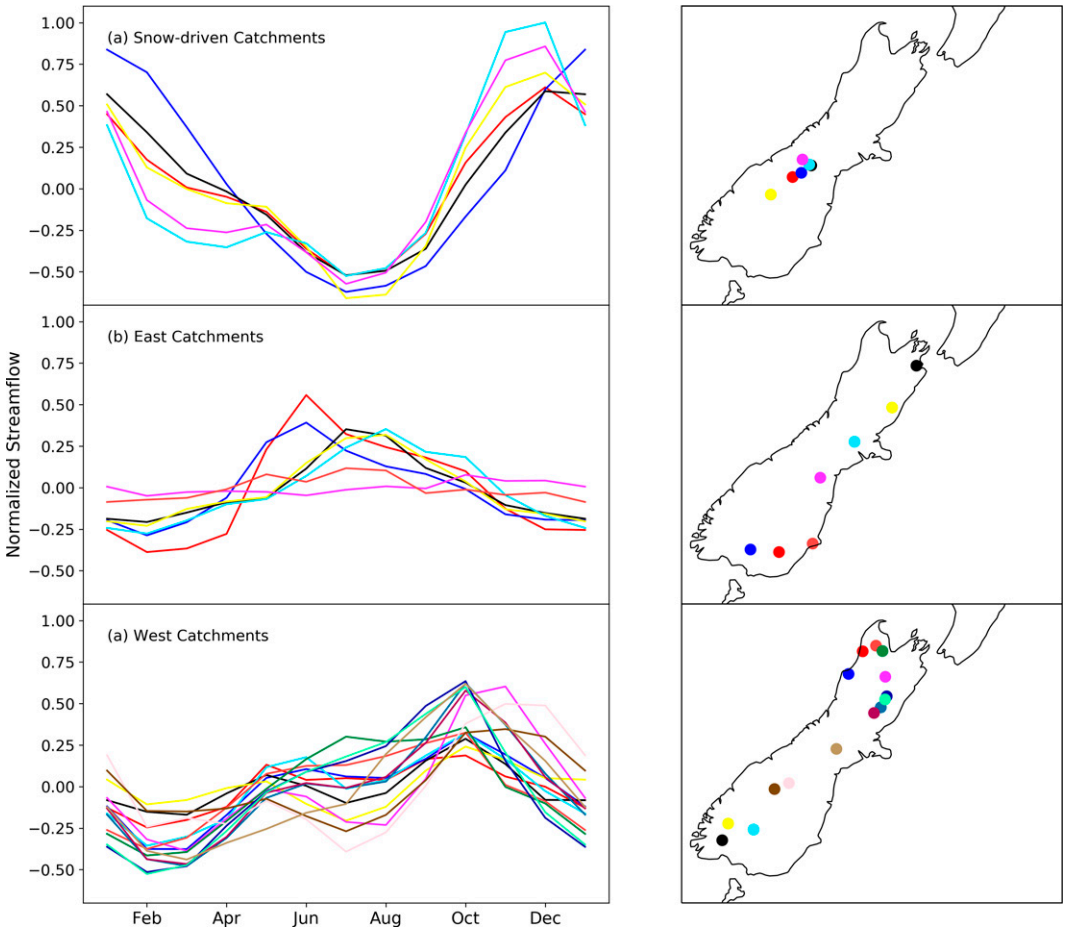

FIG. 5. Annual cycles of normalized streamflow averaged over period 1969–2019 of South Island catchments.

The regional time series is the equally weighted average of the normalized records in each region defined in Fig. 4. Note that four regions were identified for each of winter and summer, but only two regions for each of autumn and spring, leading to a total of 12 season–region combinations. Each region is denoted by unique markers. A region's composite sites are plotted with the representative marker and colored by the magnitude of the regional trend β. The legend in each seasonal plot shows the p value corresponding to the Mann–Kendall test for each region. While regionalization reveals the coherent trends within each homogenous hydrologic region, there are no regional trends at the $p < 0.1$ significance level over the shared time window, 1969–2019, where this time window was dictated by the record with the shortest duration. Over this period, the strongest trends are increasing winter west South Island streamflow ($p = 0.11$) and decreasing eastern spring streamflow ($p = 0.14$).

Figure 7 shows a multitemporal analysis, which uses as much data as possible to assess long-term hydrologic trends and provide greater insight into the usefulness of the regionalization approach. Trends are assessed over the full regional time series which begins on the date at least three records are active in the region, and trend significance is tested considering a series of start years. For each season and region, the LOWESS smoothed trend for the composite records are plotted in blue and the regional average of these records, from the date at least three records are active, is plotted in black. The p value results of trend tests considering a sequence of start dates is shown in the red/green plots, with red denoting p values greater than 0.2, dark green $0.1 < p < 0.2$, and light green $p < 0.1$. The results of the multitemporal regional trend analysis are summarized in Table 1.

The multitemporal analysis reveals the strong influence of decadal variability in NZ hydrology, highlighting that in many regions and seasons, more than 50 years of data are needed to assess long-term trends. Decadal variability across records, namely, the streamflow peak within 1969–2019, reveals the pitfalls of assessing long-term linear trends over any fixed time window around this time frame, as window selection alone could determine trend direction, magnitude, and significance. By using the maximum amount of data available in each region, however, Fig. 7 shows several regional trends with stable statistical significance over a range of start years.

Winter has the largest trend magnitudes and greatest statistical significance. The west South Island region has a significant positive trend with a β of 0.012 and p value of 0.00. This

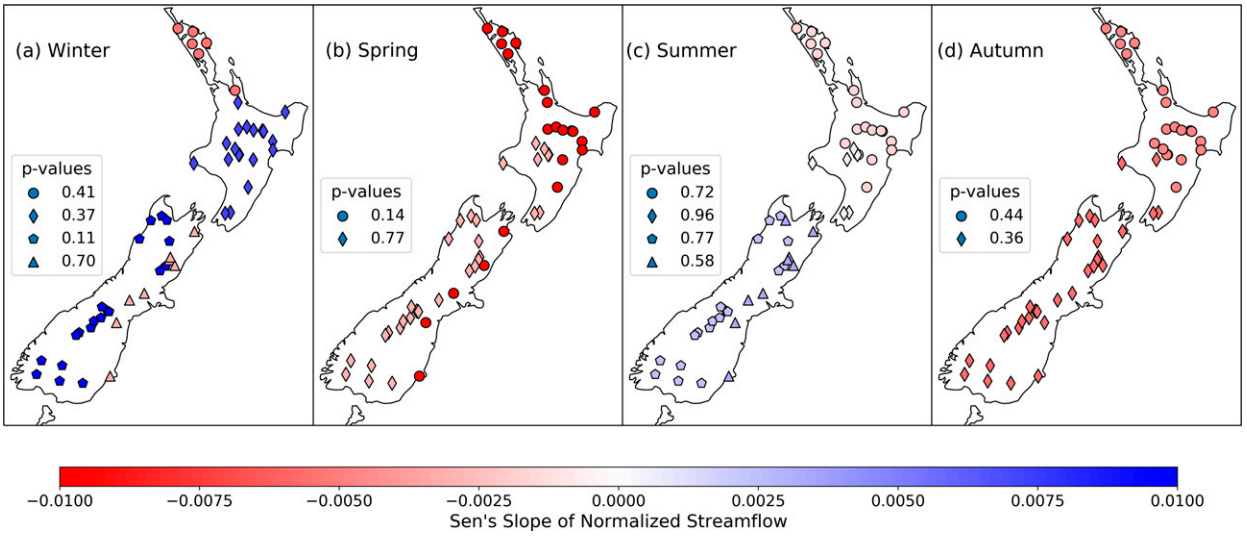

FIG. 6. Seasonal Mann–Kendall trend results for regional time series, the average of a region's normalized composite records, over the shared time window 1969–2019. Regions are denoted by unique symbols, with the regional trend magnitude β depicted through color at each composite site and the statistical significance for each regional trend shown in the legend.

region contains many lake inflow records which begin in 1932; the extended length of these records contributes to stability of the significance of the region's trend over many decades. Northland has a significant decreasing trend with a β of -0.012 and p value of 0.03, stable for several choices of start dates. Central North Island and east South Island have slight nonsignificant decreasing trends in winter streamflow, with β values of -0.006 and -0.002 and p values of 0.25 and 0.83, respectively.

Summer shows little change in streamflow for the South Island and significantly decreasing streamflow in the north North Island ($\beta = -0.008, p = 0.095$), with significance stable over a decade of start dates (Fig. 7e). The other regional results are as follows: south North Island ($\beta = -0.003, p = 0.69$), west South Island ($\beta = -0.002, p = 0.54$), and east South Island ($\beta = 0.000, p = 0.9$).

In spring, streamflow has decreased in the eastern region of the country ($\beta = -0.006, p = 0.19$) and increased in the west region ($\beta = 0.003, p = 0.37$). While the eastern region result is not significant considering the start date on which three records are active, p values are consistently below 0.2 and occasionally below 0.1 for decades of start dates (Fig. 7k). Autumn streamflow has decreased nationwide (north $\beta = -0.007$, $p = 0.11$; south $\beta = -0.005, p = 0.17$).

d. Correlations

Local detrended seasonal streamflow is correlated to zonal and meridional wind indices, local total precipitation and snowfall as represented in ERA5 (Fig. 8). Results are displayed by season along each row and by index along each column. If the local result is significant at the $p < 0.15$ level, the marker is colored by the Pearson's r correlation value between the detrended streamflow and index time series. Locations with p values above 0.15 are plotted as empty circles. The color bar ranges from -0.6 to 0.6 with warm colors as negative values and cool colors as positive values.

Zonal flow (Figs. 8a–d) across the mountainous spine of NZ correlates positively with west South Island streamflow, particularly in the winter (Fig. 8a) and spring (Fig. 8b), and negatively with eastern streamflow, particularly in summer (Fig. 8c). Meridional flow (Figs. 8e–h) has a weaker influence, correlating positively only with the far south South Island in winter (Fig. 8e) and spring (Fig. 8f) and negatively with the north North Island in spring (Fig. 8f) and summer (Fig. 8g). Total precipitation (Figs. 8i–l) correlates positively throughout the country, with larger correlations occurring in spring (Fig. 8j) and in autumn in the North Island (Fig. 8l). Notably, total precipitation does not significantly correlate with streamflow in all locations, with consistent noncorrelations in the northwest corner of the South Island in most seasons. Snowfall (Figs. 8m–p), correlates positively to spring South Island streamflow (Fig. 8n), including the snow-driven alpine catchments shown in Fig. 5a, and positively with select east South Island catchments in autumn (Fig. 8p). Caveats to these seasonal snowfall correlations due to ERA5 biases are explored in Fig. 9 and discussed below.

To assess the role of snowmelt in driving seasonal NZ streamflow behavior in alpine catchments, monthly ERA5 snow-related hydrological components and total runoff are compared to observed monthly streamflow in Fig. 9. Annual cycles of monthly values averaged over the period 1969–2019 are plotted for 1) observed streamflow and ERA5 runoff and 2) ERA5 snow depth, snowfall, snowmelt, runoff, and rainfall. Observed and ERA5 time series are averaged over the snow-driven alpine catchments shown in Fig. 5a.

ERA5 runoff in these alpine catchments has a small autumn peak and large spring speak, whereas observed streamflow in this region peaks singularly in summer (Fig. 9a), suggesting snowmelt may not play as dominant a role in

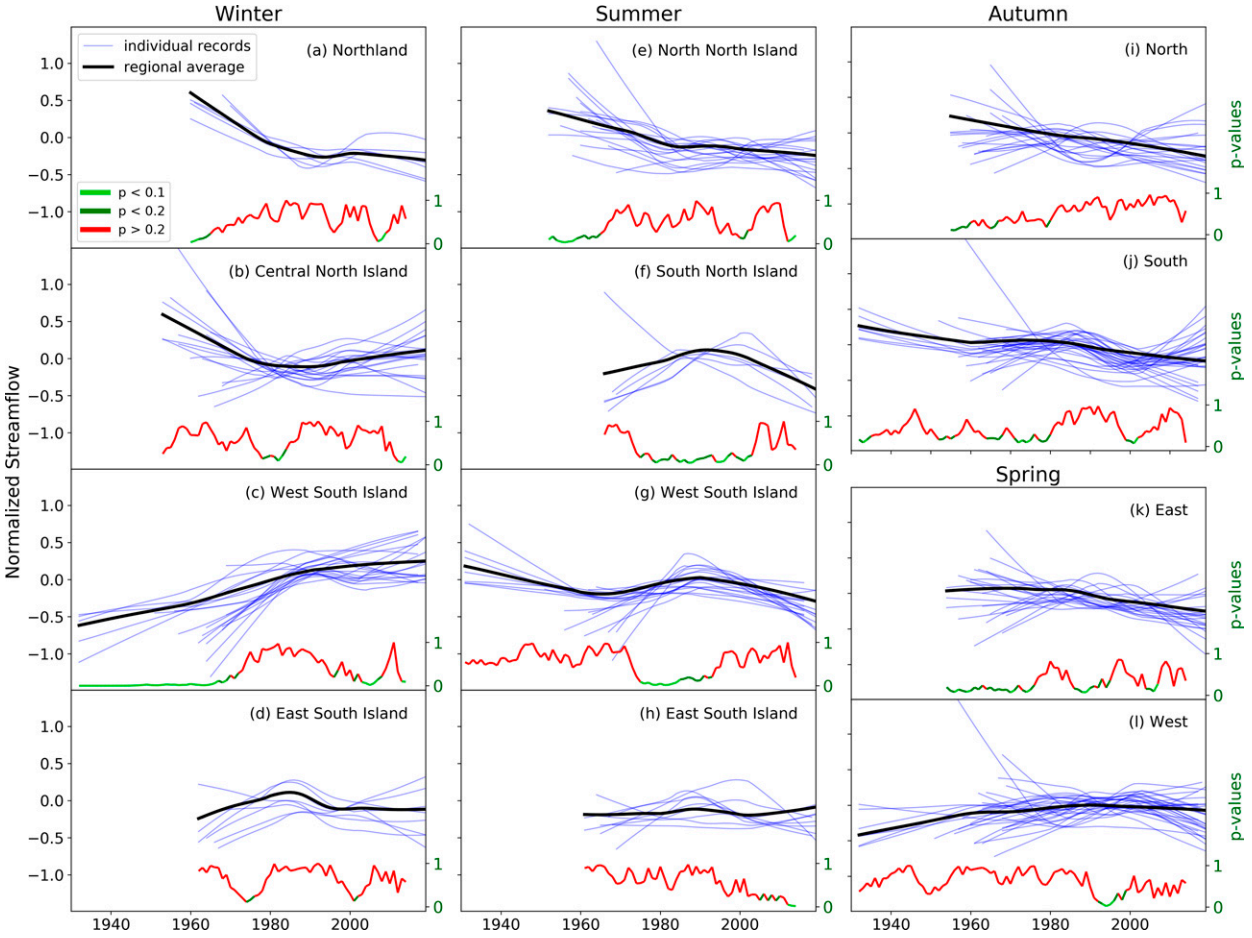

FIG. 7. Regional streamflow time series by season and region are shown in black. Individual composite records are shown in blue, starting on the date at least three records are active. All time series are smoothed with a LOWESS curve. The Mann–Kendall p values are plotted red ($p > 0.2$), dark green ($0.1 < p < 0.2$), and light green ($p < 0.1$) for tests considering a sequence of start dates.

driving runoff in ERA5 as it does in observed streamflow. The spring peak of ERA5 runoff is due to both rainfall increasing and snowmelt peaking in spring (Fig. 9b), but overall, the annual cycle is consistent with the seasonal behavior of the southern storm track with flow peaking in the autumn and spring just like the other west South Island catchments shown in Fig. 5c. While snowmelt does influence the timing and magnitude of runoff in these alpine catchments in ERA5, the timing is shifted months earlier than in the observed streamflow. This is possibly due to 1) too little snowfall and snowpack, related to reduced elevation peaks along the Southern Alps, and/or 2) timing of warming causing the snow to melt too fast.

4. Discussion and conclusions

We have identified trends and patterns of seasonality in observed near-natural NZ streamflow, and spatial patterns of correlations between streamflow and dynamic and thermodynamic climate indices. Over the last 50+ years, winter streamflow has significantly increased in the west South Island and has significantly decreased in the north North Island; summer streamflow has significantly decreased for most of the North Island; autumn streamflow has generally decreased nationwide; and spring streamflow has increased along the west coast and decreased along the east coast.

Averaging records within broadly homogenous hydrologic regions increases the signal-to-noise ratio by cancelling locally specific variations while not affecting the overall regional signal shared between the records. Hence, significant regional trends may emerge from a collection of insignificant local trends. Individual records, particularly those in near-natural benchmark networks which tend to be limited to smaller, remote catchments, are noisy and subject to several sources of uncertainty. For example, NZ rivers are very dynamic and insufficient updating of rating curves after large storms could generate spurious trends in any one station. The lake inflows are calculated from extremely accurate measures of outflow, but are used under the assumption that lake outlets have become stable such that at each lake a constant relationship exists between the level and the outflow. We assume that for these records unaccounted for short time-scale processes, like seiching, become negligible when the records are averaged over long, seasonal time scales.

TABLE 1. Regional trend results for each season and region based on regional time series which begin on the year at least three records in the region are active. Each regional time series covers a different time window, using the earliest possible start date to discern long-term trends.

Season	Region	Time window	Sen's slope	p value
Winter	Northland	1960–2019	−0.012	0.033
	Central North Island	1953–2019	−0.006	0.251
	West South Island	1932–2019	0.012	0.000
	East South Island	1962–2019	−0.002	0.830
Spring	East	1954–2019	−0.006	0.192
	West	1932–2019	0.003	0.373
Summer	North North Island	1952–2019	−0.008	0.095
	South North Island	1966–2019	−0.003	0.698
	West South Island	1931–2019	−0.002	0.545
	East South Island	1961–2019	0.000	0.896
Autumn	North	1955–2019	−0.007	0.114
	South	1932–2019	−0.005	0.167

The seasonal regions of homogenous hydrologic behavior we have defined based on PCA and SOM cluster methods are consistent with existing climate regions based on temperature and precipitation (Mullan 1998; Salinger 1980) and can be largely explained by orographic control on NZ rainfall and the seasonal placement and strength of the southern storm track (Ackerley and Renwick 2010; Nakamura and Shimpo 2004; Simmonds and Keay 2000; Trenberth 1991). The SOM method is most often used in hydrologic regionalization for the estimation of ungauged catchments or flood frequency analysis, as opposed to defining homogenous hydrologic regions based on streamflow variability, so the input data layer usually contains catchment characteristics or parameterizations of streamflow and not full streamflow time series (Di Prinzio et al. 2011; Hsu and Li 2010; Lauzon et al. 2006; Ley et al. 2011; Sharghi et al. 2018; Toth 2013). Our application of SOMs to define homogenous regions using unsmoothed, normalized seasonal streamflow time series alone successfully resulted in broadly homogenous regions consistent with the PCA regionalization and existing NZ climate regions. Our results show promise for the use of this method in defining homogenous hydrologic regions in places where orography controls much of the regionalization. Our broad regionalization here motivates further study into the characteristics of the hydrologic regions as well as the role geology and other controls may play in the regionalization of NZ hydrology.

Taking a multitemporal approach for regional trend analysis by using as much data as possible for each region and fitting trends to a series of start dates reveals the significant influence of decadal variability in NZ hydrology and the need to consider longer time windows to discern long-term trends (Lawrence et al. 2022). Natural variability, like ENSO and the IPO, or ozone changes may be causing the observed nonlinear decadal variability, namely, the streamflow peak within the period 1969–2019. This nonlinear pattern is particularly prevalent in summer streamflow, while winter contains the most secular trends (Figs. 2, 7). Due to this decadal variability, long-term trend analyses over fixed periods, like the analysis shown in Fig. 6 for the 1969–2019 period, may give misleading results dominated by decadal variability as opposed to a long-term trend signal. For example, local results of summer streamflow trends in the north North Island are largely positive over the 1969–2019 period (Fig. 3), but when the record lengths are extended in the multitemporal regional analysis, the influence of decadal variability is reduced and an overall decreasing trend emerges for many catchments resulting in a significantly decreasing regional trend (Fig. 7). Increasing winter flow in the west South Island, decreasing winter flow in the north North Island, decreasing summer flow in the North Island, and decreasing spring flow in the east are significant trends consistent over time.

Correlation patterns between zonal wind and seasonal streamflow suggest circulation is a driving factor in hydrologic behavior. Consistencies between the observed streamflow trends and known circulation changes suggest regional impacts of climate change on NZ hydrology. West South Island streamflow correlates positively with zonal winds and the significant increasing winter trends in this region are consistent with documented trends in rainfall and the strengthening and poleward shift of the southern storm track (Bender et al. 2012; Yin 2005). As storm track changes and the rainfall gradient across the Southern Alps intensify further, a significant decrease of east South Island streamflow may also emerge. Negative correlations between winter and summer North Island streamflow and zonal wind supports the connection between decreasing winter and summer North Island trends and the strengthening and poleward shift of the southern storm track.

Snowmelt also plays a role in driving hydrologic behavior in select NZ alpine catchments in the South Island, suggesting that thermodynamic climate change may also be impacting streamflow in this region. Increasing winter streamflow trends in snow-driven catchments could be caused by circulation changes increasing precipitation in winter as well as thermodynamics changes shifting winter snowfall to rainfall and causing earlier snowmelt. Increased temperatures reducing snowpack and increasing spring rain-on-snow events, which can lead to flooding and large snowpack loss (Surfleet and Tullos 2013; Zierl and Bugmann 2005), could lead to a shift in the annual cycle of snow-driven catchments. The observed seasonality (summer peak) of the snow-driven catchments, however, has not changed significantly throughout the record length, 1932–2019 (not shown). Biases in ERA5 snowfall magnitude and snowmelt timing (Fig. 9) caveat seasonal correlations between observed streamflow and ERA5 snowfall, as ERA5 appears to underestimate snowpack and overestimate the rate of snowmelt, leading to an earlier runoff timing than in the observed streamflow. Other thermodynamic influences include intensified storms due to greater water holding capacity of the atmosphere (Trenberth 2011). Finally, long-term changes in evaporation and infiltration could also contribute to the observed streamflow trends. Increasing evaporation due to increasing temperatures, particularly in summer, may contribute to all observed decreasing streamflow trends. Changes to infiltration, such as groundwater extraction for irrigation, may contribute to streamflow trends, though our near-natural records have been deliberately chosen to minimize

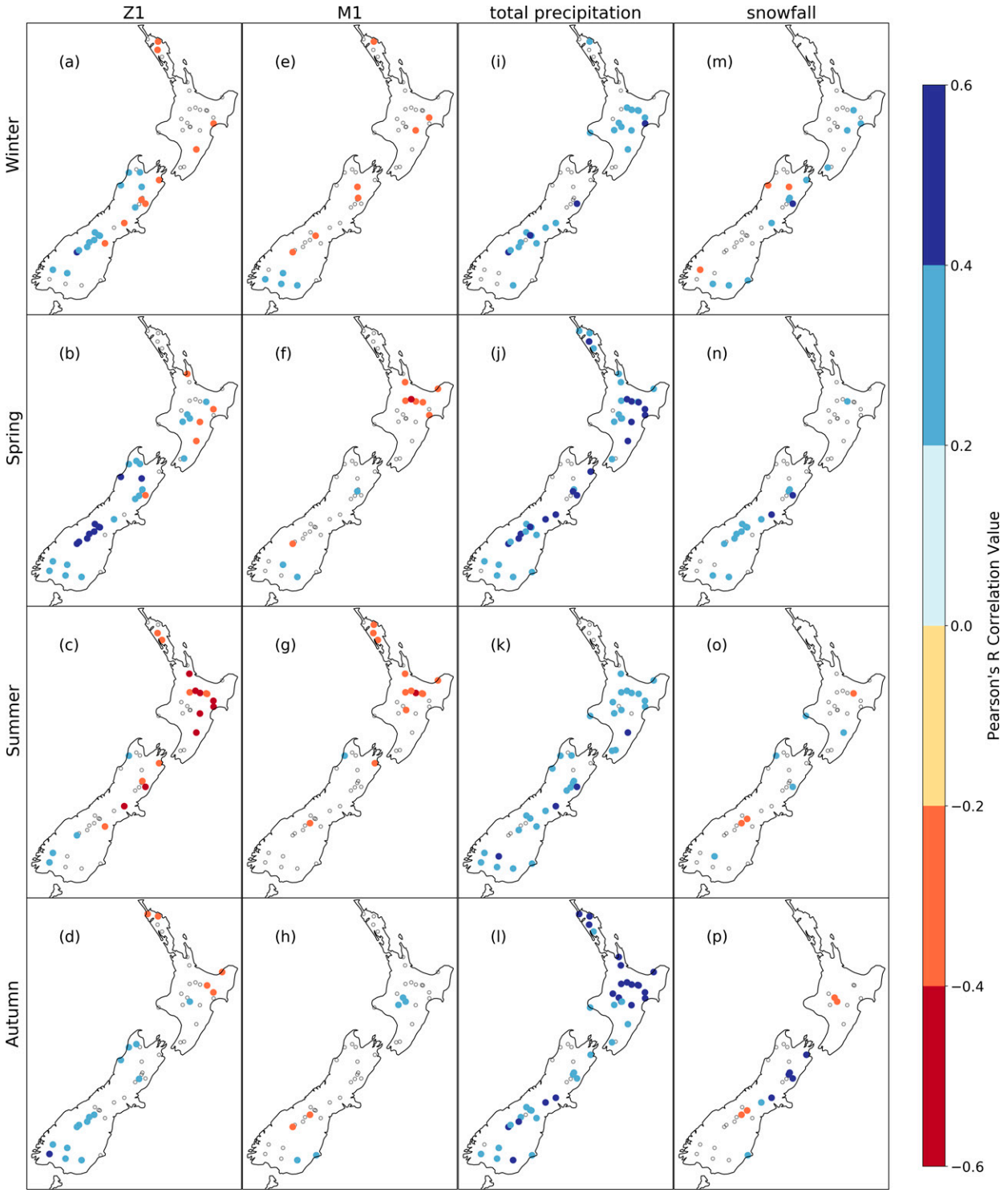

FIG. 8. Pearson's R correlations between detrended streamflow and zonal wind (Z1), meridional wind (M1), total precipitation, and snowfall as depicted in the ERA5 reanalysis. ERA5 total precipitation and snowfall is bilinearly interpolated and masked by catchment shapes to be compared to the observed streamflow. Results at an $p < 0.15$ significance level are colored, while results with p values > 0.15 are plotted as empty circles.

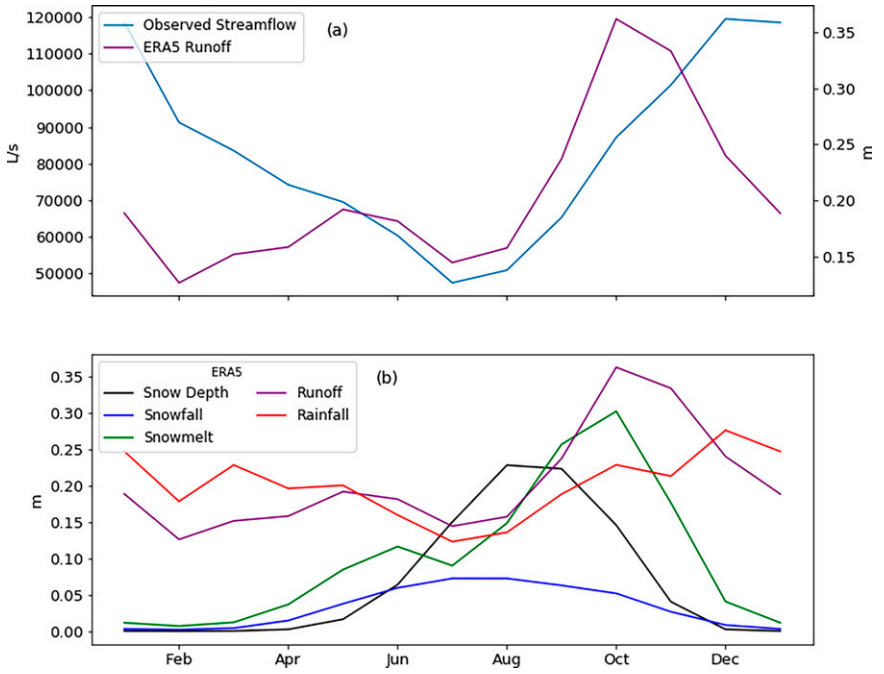

FIG. 9. Annual cycles of monthly values averaged over the period 1969–2019 are plotted for (a) observed streamflow and ERA5 runoff and (b) ERA5 snow depth, snowfall, snowmelt, runoff, and rainfall. Observed and ERA5 time series are averaged over the snow-driven alpine catchments shown in Fig. 5a. January is repeated after December for clarity.

this. Analysis using a model that includes evaporation and infiltration estimates would be needed to disentangle the relative importance of precipitation changes versus increased evaporation and infiltration to the observed streamflow trends.

The pattern of correlations discussed here, between observed streamflow and dynamic and thermodynamic indices, together with consistencies between observed trends and known shifts in large-scale circulation (Bender et al. 2012; Harrington and Renwick 2014; Yin 2005) and temperature changes (Dean and Stott 2009; Mullan 2012), point to both dynamic and thermodynamic climate change impacts on regional hydrology in NZ. While this study presents climate-driven trends in near-natural streamflow, future attribution work is needed to determine to what extent the trends are driven by natural variability, natural climate change factors (like volcanic eruptions, solar fluctuations), or anthropogenic climate change factors (changes in greenhouse gases and stratospheric ozone).

Acknowledgments. This work was supported by the Ministry of Business, Innovation and Employment (MBIE) of Aotearoa New Zealand through the Endeavour programme's Whakahura: Extreme Events and the Emergence of Climate Change project, and the Victoria University of Wellington through a doctoral scholarship.

Data availability statement. Streamflow records used in this study are funded severally by NIWA, MBIE, regional councils and power companies and may be available through these entities or by contacting the authors.

APPENDIX

Mann–Kendall (MK) Test and Sen's Slope

The Mann–Kendall statistic S measures association between rankings by considering the number of concordant and discordant pairs in a series:

$$S = \sum_{i=1}^{n-1} \sum_{j=i+1}^{n} \text{sign}(y_j - y_i),$$

$$\text{sign}(y_j - y_i) = \begin{cases} 1, & \text{if } y_j - y_i > 0 \\ 0, & \text{if } y_j - y_i = 0 \\ -1, & \text{if } y_j - y_i < 0 \end{cases},$$

where n is the length of the sample and y_i and y_j are from $i = 1, 2, \ldots, n-1$ and $j = k+1, \ldots, n$. If n is bigger than 8, S approximates to normal distribution, with a mean of 0 and variance of S can be acquired as follows:

$$\text{var}(S) = \frac{n(n-1)(2n+5)}{18}.$$

The test statistic Z is then

$$Z = \begin{cases} \dfrac{S-1}{\sqrt{\text{var}(S)}}, & \text{if } S > 0 \\ 0, & \text{if } S = 0 \\ \dfrac{S+1}{\sqrt{\text{var}(S)}}, & \text{if } S < 0 \end{cases},$$

where $Z > 0$ denotes an increasing trend, $Z < 0$ a decreasing trend, and $Z = 0$ no trend. Given a confidence level, α, the null hypothesis is rejected if the absolute value of Z is larger than the theoretical value $Z_{1-\alpha/2}$ (two-tailed test).

The magnitude of the linear trend detected by the MK test can be estimated by the Sen's slope,

$$\beta = \text{median}\left(\frac{x_j - x_i}{j - i}\right),\ j > i,$$

where $\beta > 0$ indicates an increasing trend, $\beta < 0$ a decreasing trend, and $\beta = 0$ no trend.

REFERENCES

Aawar, T., D. Khare, and L. Singh, 2019: Identification of the trend in precipitation and temperature over the Kabul River subbasin: A case study of Afghanistan. *Model. Earth Syst. Environ.*, **5**, 1377–1394, https://doi.org/10.1007/s40808-019-00597-9.

Ackerley, D., and J. A. Renwick, 2010: The Southern Hemisphere semiannual oscillation and circulation variability during the mid-Holocene. *Climate Past*, **6**, 415–430, https://doi.org/10.5194/cp-6-415-2010.

Bender, F. A.-M., V. Ramanathan, and G. Tselioudis, 2012: Changes in extratropical storm track cloudiness 1983–2008: Observational support for a poleward shift. *Climate Dyn.*, **38**, 2037–2053, https://doi.org/10.1007/s00382-011-1065-6.

Birsan, M.-V., P. Molnar, P. Burlando, and M. Pfaundler, 2005: Streamflow trends in Switzerland. *J. Hydrol.*, **314**, 312–329, https://doi.org/10.1016/j.jhydrol.2005.06.008.

——, L. Zaharia, V. Chendes, and E. Branescu, 2014: Seasonal trends in Romanian streamflow. *Hydrol. Processes*, **28**, 4496–4505, https://doi.org/10.1002/hyp.9961.

Burn, D. H., 2008: Climatic influences on streamflow timing in the headwaters of the Mackenzie River Basin. *J. Hydrol.*, **352**, 225–238, https://doi.org/10.1016/j.jhydrol.2008.01.019.

——, and M. A. Hag Elnur, 2002: Detection of hydrologic trends and variability. *J. Hydrol.*, **255**, 107–122, https://doi.org/10.1016/S0022-1694(01)00514-5.

Chauluka, F., S. Singh, and R. Kumar, 2021: Rainfall and streamflow trends of Thuchila River, Southern Malawi. *Mater. Today Proc.*, **34**, 846–855, https://doi.org/10.1016/j.matpr.2020.06.228.

Chen, Y., Y. Guan, G. Shao, and D. Zhang, 2016: Investigating trends in streamflow and precipitation in Huangfuchuan basin with wavelet analysis and the Mann-Kendall test. *Water*, **8**, 77, https://doi.org/10.3390/w8030077.

Collins, D. B. G., 2020: New Zealand river hydrology under late 21st century climate change. *Water*, **12**, 2175, https://doi.org/10.3390/w12082175.

——, 2021: Hydrological sentinels and the relative emergence of climate change signals in New Zealand river flows. *Hydrol. Sci. J.*, **66**, 2146–2154, https://doi.org/10.1080/02626667.2021.1987439.

Dean, S. M., and P. A. Stott, 2009: The effect of local circulation variability on the detection and attribution of New Zealand temperature trends. *J. Climate*, **22**, 6217–6229, https://doi.org/10.1175/2009JCLI2715.1.

Di Prinzio, M., A. Castellarin, and E. Toth, 2011: Data-driven catchment classification: Application to the PUB problem. *Hydrol. Earth Syst. Sci.*, **15**, 1921–1935, https://doi.org/10.5194/hess-15-1921-2011.

Dixon, H., D. M. Lawler, and A. Y. Shamseldin, 2006: Streamflow trends in western Britain. *Geophys. Res. Lett.*, **33**, L19406, https://doi.org/10.1029/2006GL027325.

Douville, H., and Coauthors, 2021: Water cycle changes. *Climate Change 2021: The Physical Science Basis*, V. Masson-Delmotte et al., Eds., Cambridge University Press, 1055–1210.

Dravitzki, S., and J. McGregor, 2011: Extreme precipitation of the Waikato region, New Zealand. *Int. J. Climatol.*, **31**, 1803–1812, https://doi.org/10.1002/joc.2189.

Gautam, M. R., and K. Acharya, 2012: Streamflow trends in Nepal. *Hydrol. Sci. J.*, **57**, 344–357, https://doi.org/10.1080/02626667.2011.637042.

Gilbert, D. J., 1978: Calculating lake inflow (note). *J. Hydrol.*, **17**, 39–43,

Gudmundsson, L., M. Leonard, H. X. Do, S. Westra, and S. I. Seneviratne, 2019: Observed trends in global indicators of mean and extreme streamflow. *Geophys. Res. Lett.*, **46**, 756–766, https://doi.org/10.1029/2018GL079725.

——, and Coauthors, 2021: Globally observed trends in mean and extreme river flow attributed to climate change. *Science*, **371**, 1159–1162, https://doi.org/10.1126/science.aba3996.

Guetter, A. K., and K. P. Georgakakos, 1993: River outflow of the conterminous United States, 1939–1988. *Bull. Amer. Meteor. Soc.*, **74**, 1873–1892, https://doi.org/10.1175/1520-0477(1993)074<1873:ROOTCU>2.0.CO;2.

Gumus, V., Y. Avsaroglu, and O. Simsek, 2022: Streamflow trends in the Tigris River basin using Mann-Kendall and innovative trend analysis methods. *J. Earth Syst. Sci.*, **131**, 34, https://doi.org/10.1007/s12040-021-01770-4.

Hannaford, J., G. Buys, K. Stahl, and L. M. Tallaksen, 2013: The influence of decadal-scale variability on trends in long European streamflow records. *Hydrol. Earth Syst. Sci.*, **17**, 2717–2733, https://doi.org/10.5194/hess-17-2717-2013.

——, N. Mastrantonas, G. Vesuviano, and S. Turner, 2021: An updated national-scale assessment of trends in UK peak river flow data: How robust are observed increases in flooding? *Hydrol. Res.*, **52**, 699–718, https://doi.org/10.2166/nh.2021.156.

Harrigan, S., J. Hannaford, K. Muchan, and T. J. Marsh, 2018: Designation and trend analysis of the updated UK Benchmark Network of river flow stations: The UKBN2 dataset. *Hydrol. Res.*, **49**, 552–567, https://doi.org/10.2166/nh.2017.058.

Harrington, L., and J. Renwick, 2014: Secular changes in New Zealand rainfall characteristics 1950–2009. *Wea. Climate*, **34**, 50–59, https://doi.org/10.2307/26169744.

Henderson, R. D., and S. M. Thompson, 1999: Extreme rainfalls in the Southern Alps of New Zealand. *J. Hydrol.*, **38**, 309–330.

Hersbach, H., and Coauthors, 2020: The ERA5 global reanalysis. *Quart. J. Roy. Meteor. Soc.*, **146**, 1999–2049, https://doi.org/10.1002/qj.3803.

Hirabayashi, Y., R. Mahendran, S. Koirala, L. Konoshima, D. Yamazaki, S. Watanabe, H. Kim, and S. Kanae, 2013: Global flood risk under climate change. *Nat. Climate Change*, **3**, 816–821, https://doi.org/10.1038/nclimate1911.

Hsu, K.-C., and S.-T. Li, 2010: Clustering spatial–temporal precipitation data using wavelet transform and self-organizing map neural network. *Adv. Water Resour.*, **33**, 190–200, https://doi.org/10.1016/j.advwatres.2009.11.005.

Hu, Z., S. Liu, G. Zhong, H. Lin, and Z. Zhou, 2020: Modified Mann-Kendall trend test for hydrological time series under the scaling hypothesis and its application. *Hydrol. Sci. J.*, **65**, 2419–2438, https://doi.org/10.1080/02626667.2020.1810253.

Hussain, M., and I. Mahmud, 2019: pyMannKendall: A python package for non parametric Mann Kendall family of trend

tests. *J. Open Source Software*, **4**, 1556, https://doi.org/10.21105/joss.01556.

Jencso, K. G., B. L. McGlynn, M. N. Gooseff, S. M. Wondzell, K. E. Bencala, and L. A. Marshall, 2009: Hydrologic connectivity between landscapes and streams: Transferring reach- and plot-scale understanding to the catchment scale. *Water Resour. Res.*, **45**, W04428, https://doi.org/10.1029/2008WR007225.

Kalteh, A. M., P. Hjorth, and R. Berndtsson, 2008: Review of the self-organizing map (SOM) approach in water resources: Analysis, modelling and application. *Environ. Modell. Software*, **23**, 835–845, https://doi.org/10.1016/j.envsoft.2007.10.001.

Kendall, M. G., 1975: *Rank Correlation Methods*. 4th ed. Charles Griffin, 202 pp.

Kohonen, T., 1990: The self-organizing map. *Proc. IEEE*, **78**, 1464–1480, https://doi.org/10.1109/5.58325.

Konapala, G., A. K. Mishra, Y. Wada, and M. E. Mann, 2020: Climate change will affect global water availability through compounding changes in seasonal precipitation and evaporation. *Nat. Commun.*, **11**, 3044, https://doi.org/10.1038/s41467-020-16757-w.

Lauzon, N., F. Anctil, and C. W. Baxter, 2006: Clustering of heterogeneous precipitation fields for the assessment and possible improvement of lumped neural network models for streamflow forecasts. *Hydrol. Earth Syst. Sci.*, **10**, 485–494, https://doi.org/10.5194/hess-10-485-2006.

Lawrence, J., and Coauthors, 2022: Australasia. *Climate Change 2022: Impacts, Adaptation and Vulnerability*, H.-O. Pörtner et al., Eds., Cambridge University Press, 1581–1688.

Ley, R., M. C. Casper, H. Hellebrand, and R. Merz, 2011: Catchment classification by runoff behavior with self-organizing maps (SOM). *Hydrol. Earth Syst. Sci.*, **15**, 2947–2962, https://doi.org/10.5194/hess-15-2947-2011.

Lin, G.-F., and L.-H. Chen, 2006: Identification of homogeneous regions for regional frequency analysis using the self-organizing map. *J. Hydrol.*, **324** (1–4), 1–9, https://doi.org/10.1016/j.jhydrol.2005.09.009.

Lins, H. F., 1997: Regional streamflow regimes and hydroclimatology of the United States. *Water Resour. Res.*, **33**, 1655–1667, https://doi.org/10.1029/97WR00615.

——, and J. R. Slack, 2005: Seasonal and regional characteristics of U.S. streamflow trends in the United States from 1940 to 1999. *Phys. Geogr.*, **26**, 489–501, https://doi.org/10.2747/0272-3646.26.6.489.

Mallick, J., S. Talukdar, M. Alsubih, R. Salam, M. Ahmed, N. B. Kahla, and M. Shamimuzzaman, 2021: Analysing the trend of rainfall in Asir region of Saudi Arabia using the family of Mann-Kendall tests, innovative trend analysis, and detrended fluctuation analysis. *Theor. Appl. Climatol.*, **143**, 823–841, https://doi.org/10.1007/s00704-020-03448-1.

Mann, H. B., 1945: Nonparametric tests against trend. *Econometrica*, **13**, 245–259, https://doi.org/10.2307/1907187.

Maurer, E. P., D. P. Lettenmaier, and N. J. Mantua, 2004: Variability and potential sources of predictability of North American runoff. *Water Resour. Res.*, **40**, W09306, https://doi.org/10.1029/2003WR002789.

Milly, P. C. D., K. A. Dunne, and A. V. Vecchia, 2005: Global pattern of trends in streamflow and water availability in a changing climate. *Nature*, **438**, 347–350, https://doi.org/10.1038/nature04312.

Ministry of Business, Innovation and Employment, 2021: Table 1: Yearly electricity generation, consumption, & lines losses (GWh). Accessed 25 October 2021, https://www.mbie.govt.nz/building-and-energy/energy-and-natural-resources/energy-statistics-and-modelling/energy-statistics/electricity-statistics/.

Mullan, A. B., 1998: Southern Hemisphere sea-surface temperatures and their contemporary and lag association with New Zealand temperature and precipitation. *Int. J. Climatol.*, **18**, 817–840, https://doi.org/10.1002/(SICI)1097-0088(19980630)18:8<817::AID-JOC261>3.0.CO;2-E.

——, 2012: Applying the Rhoades and Salinger method to New Zealand's "seven-station" temperature series. *Wea. Climate*, **32**, 23–37, https://doi.org/10.2307/26169723.

Nakamura, H., and A. Shimpo, 2004: Seasonal variations in the Southern Hemisphere storm tracks and jet streams as revealed in a reanalysis dataset. *J. Climate*, **17**, 1828–1844, https://doi.org/10.1175/1520-0442(2004)017<1828:SVITSH>2.0.CO;2.

Nayak, A., D. Marks, D. G. Chandler, and M. Seyfried, 2010: Long-term snow, climate, and streamflow trends at the Reynolds Creek Experimental Watershed, Owyhee Mountains, Idaho, United States. *Water Resour. Res.*, **46**, W06519, https://doi.org/10.1029/2008WR007525.

Pirooz, A. A. S., S. Moore, T. Carey-Smith, R. Turner, and C. H. Su, 2021: Evaluation of global and regional reanalyses performance over New Zealand. *Wea. Climate*, **41**, 52–71, https://doi.org/10.2307/27127989.

Prince, H. D., N. J. Cullen, P. B. Gibson, J. Conway, and D. G. Kingston, 2021: A climatology of atmospheric rivers in New Zealand. *J. Climate*, **34**, 4383–4402, https://doi.org/10.1175/JCLI-D-20-0664.1.

Purdy, J. C., and G. L. Austin, 2003: The role of synoptic cloud in orographic rainfall in the Southern Alps of New Zealand. *Meteor. Appl.*, **10**, 355–365, https://doi.org/10.1017/S1350482703001087.

Reback, J., and Coauthors, 2020: Pandas-dev/pandas: Pandas 1.0.3. Zenodo, accessed 15 June 2021, https://doi.org/10.5281/zenodo.3715232.

Riese, F. M., S. Keller, and S. Hinz, 2020: Supervised and semi-supervised self-organizing maps for regression and classification focusing on hyperspectral data. *Remote Sens.*, **12**, 7, https://doi.org/10.3390/rs12010007.

Salinger, M. J., 1980: New Zealand climate: I. Precipitation patterns. *Mon. Wea. Rev.*, **108**, 1892–1904, https://doi.org/10.1175/1520-0493(1980)108<1892:NZCIPP>2.0.CO;2.

——, and A. B. Mullan, 1999: New Zealand climate: Temperature and precipitation variations and their links with atmospheric circulation 1930–1994. *Int. J. Climatol.*, **19**, 1049–1071, https://doi.org/10.1002/(SICI)1097-0088(199908)19:10<1049::AID-JOC417>3.0.CO;2-Z.

Seabold, S., and J. Perktold, 2010: Statsmodels: Econometric and statistical modeling with python. *Proc. Ninth Python in Science Conf. (SciPy 2010)*, Austin, TX, The University of Texas at Austin, 57–61, https://doi.org/10.25080/Majora-92bf1922-011.

Sen, P. K., 1968: Estimates of the regression coefficient based on Kendall's Tau. *J. Amer. Stat. Assoc.*, **63**, 1379–1389, https://doi.org/10.1080/01621459.1968.10480934.

Sharghi, E., V. Nourani, S. Soleimani, and F. Sadikoglu, 2018: Application of different clustering approaches to hydroclimatological catchment regionalization in mountainous regions, a case study in Utah State. *J. Mt. Sci.*, **15**, 461–484, https://doi.org/10.1007/s11629-017-4454-4.

Shu, J., A. Y. Shamseldin, and E. Weller, 2021: The impact of atmospheric rivers on rainfall in New Zealand. *Sci. Rep.*, **11**, 5869, https://doi.org/10.1038/s41598-021-85297-0.

Simmonds, I., and K. Keay, 2000: Mean Southern Hemisphere extratropical cyclone behavior in the 40-year NCEP–NCAR reanalysis. *J. Climate*, **13**, 873–885, https://doi.org/10.1175/1520-0442(2000)013<0873:MSHECB>2.0.CO;2.

Slack, J. R., and J. M. Landwehr, 1992: Hydro-climatic Data Network (HCDN); A U.S. Geological Survey streamflow data set for the United States for the study of climate variations, 1874–1988. USGS Open-File Rep. 92-129, 193 pp., https://doi.org/10.3133/ofr92129.

Stahl, K., and Coauthors, 2010: Streamflow trends in Europe: Evidence from a dataset of near-natural catchments. *Hydrol. Earth Syst. Sci.*, **14**, 2367–2382, https://doi.org/10.5194/hess-14-2367-2010.

Surfleet, C. G., and D. D. Tullos, 2013: Variability in effect of climate change on rain-on-snow peak flow events in a temperate climate. *J. Hydrol.*, **479**, 24–34, https://doi.org/10.1016/j.jhydrol.2012.11.021.

Tait, A. B., and B. B. Fitzharris, 1998: Relationships between New Zealand rainfall and south-west Pacific pressure patterns. *Int. J. Climatol.*, **18**, 407–424, https://doi.org/10.1002/(SICI)1097-0088(19980330)18:4<407::AID-JOC256>3.0.CO;2-S.

Toth, E., 2013: Catchment classification based on characterisation of streamflow and precipitation time series. *Hydrol. Earth Syst. Sci.*, **17**, 1149–1159, https://doi.org/10.5194/hess-17-1149-2013.

Trenberth, K. E., 1976: Spatial and temporal variations of the Southern Oscillation. *Quart. J. Roy. Meteor. Soc.*, **102**, 639–653, https://doi.org/10.1002/qj.49710243310.

——, 1991: Storm tracks in the Southern Hemisphere. *J. Atmos. Sci.*, **48**, 2159–2178, https://doi.org/10.1175/1520-0469(1991)048<2159:STITSH>2.0.CO;2.

——, 2011: Changes in precipitation with climate change. *Climate Res.*, **47**, 123–138, https://doi.org/10.3354/cr00953.

——, A. Dai, G. van der Schrier, P. D. Jones, J. Barichivich, K. R. Briffa, and J. Sheffield, 2014: Global warming and changes in drought. *Nat. Climate Change*, **4**, 17–22, https://doi.org/10.1038/nclimate2067.

Vörösmarty, C. J., and D. Sahagian, 2000: Anthropogenic disturbance of the terrestrial water cycle. *BioScience*, **50**, 753–765, https://doi.org/10.1641/0006-3568(2000)050[0753:ADOTTW]2.0.CO;2.

Winter, T. C., 2001: The concept of hydrologic landscapes. *J. Amer. Water Resour. Assoc.*, **37**, 335–349, https://doi.org/10.1111/j.1752-1688.2001.tb00973.x.

Yin, J. H., 2005: A consistent poleward shift of the storm tracks in simulations of 21st century climate. *Geophys. Res. Lett.*, **32**, L18701, https://doi.org/10.1029/2005GL023684.

Zierl, B., and H. Bugmann, 2005: Global change impacts on hydrological processes in Alpine catchments. *Water Resour. Res.*, **41**, W02028, https://doi.org/10.1029/2004WR003447.